Electron Impact Fragmentation of Size-Selected Krypton Clusters

Christof Steinbach, Michal Fárník,[†] and Udo Buck*

Max-Planck Institut für Dynamik und Selbstorganisation, Bunsenstr. 10, D-37073 Göttingen, Germany

Carrie A. Brindle[‡] and Kenneth C. Janda

Department of Chemistry, University of California, Irvine, California 92697-2025

Received: April 28, 2006; In Final Form: May 31, 2006

Clusters of krypton are generated in a supersonic expansion and size selected by deflection from a helium target beam. By measuring angular distributions for different fragment masses and time-of-flight distributions for fixed deflection angles and fragment masses, the complete fragmentation patterns for electron impact ionization at 70 eV are obtained from the dimer to the heptamer. For each of the neutral Kr_n clusters studied, the main fragment is the monomer Kr^+ ion with a probability $f_{n1} > 90\%$. The probability of observing dimer Kr_2^+ ions is much smaller than expected for each initial cluster size. The trimer ion Kr_3^+ appears first from the neutral Kr_5, and its fraction increases with increasing neutral cluster size n, but is always much smaller than that of the monomer or dimer. For neutral Kr_7, all possible ion fragments are observed, but the monomer still represents 90% of the overall probability and fragments with $n > 3$ contribute less than 1% of the total. Aspects of the Kr_n cluster ionization process and the experimental measurements are discussed to provide possible reasons for the surprisingly high probability of observing fragmentation to the Kr^+ monomer ion.

I. Introduction

Rare gases are the prototypes of weakly bound systems. They were among the first examples for which a unifying description of the interaction potential was derived which covered both the gas and the condensed phase.[1] Thus it is not surprising that rare gas clusters also provide ideal systems for investigating dynamical models of the detection mechanisms of weakly bound neutral clusters upon the interaction with photon or electron impact. These processes are known to be dominated by extensive fragmentation.[2−4] The first experimental results for size selected neutral clusters were published for Ar_n clusters.[5−8] The dominant fragment channel for cluster sizes up to $n = 9$ was the dimer ion Ar_2^+, although the calculated minimum configuration was that of Ar_3^+.[9,10] The first quantitative calculation on the fragmentation probabilities confirmed the experimental findings[8] using mean field dynamics with DIM (diatomics in molecule) potential surfaces. In the meantime, much better calculations have been performed in which all potential surfaces close to the ground state and their couplings are taken into account.[11] The further applications of this improved theory were carried out for neon[12] and krypton clusters[13] to study the influence of the spin−orbit interaction.

Therefore we found it quite interesting to provide new detailed measurements of size selected neutral clusters for a direct comparison with these results. Previous experimental studies dealt with the photon and electron impact ionization of krypton clusters. The clusters were not size selected and extended in most cases to large average sizes. In photoelectron experiments using synchrotron radiation for the excitation, inner valence or core electrons were probed.[14,15] With electron impact excitation, emitted photons and metastable neutral fragments were observed.[16] The energetics and dissociation energies of *ionic* krypton clusters have also been investigated in great detail.[17−20]

In the present paper we apply the scattering method[5,6] to krypton Kr_n clusters that are ionized by electron impact ionization. We have chosen Kr_n with its heavy mass, because (a) it will be less effected by collisional dissociation in the selection process, (b) it exhibits a large spin−orbit effect, and (c) it is the first application of such a detailed fragmentation analysis to a heavy cluster. Up to now, aside from Ar_n, only a series of molecular systems of lighter masses has been investigated, including $(C_2H_4)_n$,[21] $(CO_2)_n$,[22] $(NO)_n$,[23,24] $(NH_3)_n$,[25] and $(D_2O)_n$.[26] After a detailed description of the selection process, we will present measurements of the fragmentation behavior of these size selected clusters upon electron impact ionization from $n = 2$ to 7. The results are quite different from those previously obtained for Ar_n, and also from the predictions of the latest calculations[13] in that the monomer Kr^+ ion is always by far the most probable fragment. This result is very surprising, and possible reasons for it are discussed but no unambiguous conclusions could be drawn.

II. Experimental Section

A. Crossed Beams Apparatus. The crossed beam apparatus used here has been described in detail elsewhere.[27] Briefly, the two supersonic nozzle beams are generated in two differentially pumped oven chambers that are mounted on the base platform of the scattering chamber. The beams enter this chamber through skimmers to provide well-defined beam profiles and are crossed at an angle of 90° in the scattering center. For angular dependent measurements, the complete base of the scattering chamber is rotated with respect to the scattering center, while the detector position is fixed. The detector consists of a time-of-flight (TOF)

* E-mail:ubuck@gwdg.de.
[†] Present address: J. Heyrovsky Institute of Physical Chemistry, Academy of Sciences of the Czech Republic, Prague 8, Czech Republic.
[‡] Present address: Getty Conservation Institute, 1200 Getty Center Drive, Los Angeles, CA 90049-1684.

Fragmentation of Krypton Clusters

J. Phys. Chem. A, Vol. 110, No. 29, 2006 **9109**

TABLE 1: Beam Data of the Krypton Cluster Beam and the Helium Target Beam[a]

| species	v [m/s]	$\Theta_{max}(n)$
$n = 1$	395	23.3°
$n = 2$	388	12.9°
$n = 3$	371	8.6°
$n = 4$	369	6.5°
$n = 5$	368	5.3°
$n = 6$	368	4.4°
$n = 7$	367	3.7°
helium	1740	

[a] v is the flow velocity and θ_{max} is the maximum scattering angle.
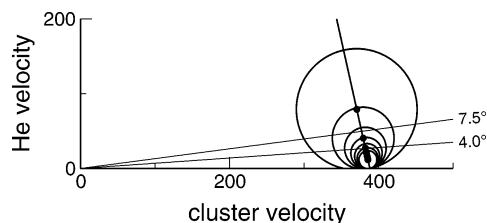
Figure 1. Newton diagram for the scattering of Kr_n by helium for $n = 1$ to 7.

spectrometer, using the pseudorandom chopping technique on a flight path of 449.5 mm, and a mass spectrometer consisting of an electron bombardment ionizer, a quadrupole rod system, and an off-axis mounted ion multiplier. The electron beam was operated at an energy of 70 eV. Either the detected ions are counted as a function of the deflection angle to derive angular distributions or the velocity is measured by TOF analysis of the scattered signal. In the early stage of the experiment, a different apparatus has been used.[7,8] The geometrical dimensions and thus the resolution were different compared to the one described here, but the mode of operation was the same.

In the present study, the clusters are produced in a supersonic expansion of the krypton gas at a backing pressure of 2.5 bar through a 60 μm conical nozzle of 6 mm length and an opening angle of 20.4°. The resulting cluster beam velocities are summarized in Table 1. They were measured at the fragment masses of the corresponding neutrals. The monomer was detected at the mass $m/z = 84$ u. For the clusters, the corresponding multiples of this value were used. The speed ratios $S = v/v_w$ of the flow velocity v to the most probable thermal velocity v_w were around 30 except for the monomer and dimer where $S = 9$ and 20, respectively, were measured. The angular deflection of the clusters was generated by a He atom beam produced in a 30 μm pinhole expansion at 30 bar (see Table 1).

B. Size Selection. As described in detail in an earlier publication,[6] the scattering analysis of a cluster beam enables us to find a unique correlation between detected cluster ions and their neutral precursors independent of the cluster size distribution in the primary beam and the fragmentation process taking place in the ion source. The method relies on the specific kinematic behavior of clusters with different sizes scattered from a target beam and is commonly described in terms of a Newton diagram as shown in Figure 1. Because of the scattering process of the Kr_n clusters with the light helium target atoms, each cluster with a certain size can be scattered into the laboratory (lab) system only within a certain angular range. This is visualized in Figure 1 by the different circles representing the final center-of-mass (cm) velocities of elastically scattered clusters. The largest circle represents the scattering of the monomer, whereas the smaller circles define the corresponding values for the cluster scattering up to the heptamer. The
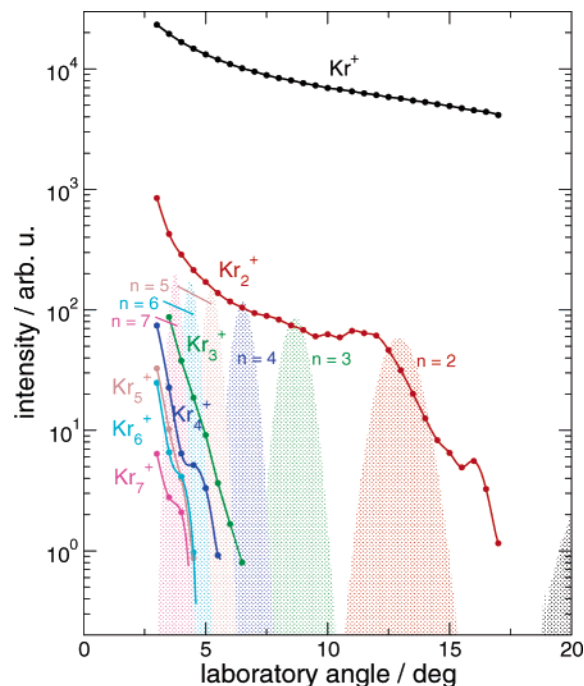
Figure 2. Measured angular dependence of scattered krypton clusters $S_k(\Theta)$ at the masses k indicated. The shaded colored areas mark the onset of the different neutral cluster sizes n.

scattering process implies that for each cluster size n a corresponding specific maximum scattering angle $\Theta_{max}(n)$ exists. Thus the selection of a specific detection angle in the lab system is acting as a "low pass filter". All larger Kr_n clusters with $n > n_{max}(\Theta)$ are excluded from being detected, since they have smaller maximum scattering angles. In the lab system, the limiting angles for the clusters from $n = 1$ to 7 are given in Table 1. Thus the measurement at a detection angle of 7.5°, as depicted in Figure 1, excludes most of the tetramer contribution, depending somewhat on the realistic velocity and angular resolution of the apparatus, and certainly excludes any contribution of pentamers to the measured ion signal (see Figure 2).

Under typical experimental conditions with moderate energy transfer during the scattering process, clusters of different sizes that are scattered in one lab angle Θ arrive with different velocities. This allows us to disentangle the various fragment contributions of the total signal S_k. To get this information, time-resolved measurements of the scattered particles are necessary. The intensity of the scattered neutral cluster of size n, at the laboratory angle Θ, final velocity v', and detected at the mass k of the mass spectrometer is given by

$$N'_{nk} = K\rho_n\sigma_n C_n f_{nk} T_k \tag{1}$$

The constant K contains the variables concerning the scattering process which are not relevant for the cluster separation, ρ_n is the cluster density, σ_n is the differential scattering cross section with the target beam in the lab system, C_n is the total ionization cross section, f_{nk} is the probability for the formation of an ion of mass k from a cluster of size n with $\Sigma_k f_{nk} = 1$, and T_k is the transmission of the mass filter. If no velocity analysis is applied, the signal $S_k(\Theta)$ is summed over all neutral cluster sizes, which may contribute at this scattering angle to the fragment mass k

$$S_k(\Theta) = \sum_{n=k}^{n_{max}(\Theta)} N_{nk} \tag{2}$$

Here we used the relation $N_{nk} = N'_{nk}/T_k$ for the transmission corrected intensities. This clearly illustrates that in the case of fragmentation during the ionization process, ionic fragments N_{nk} from neutral clusters with sizes n up to $n = n_{max}(\Theta)$ can be detected at the selected ion mass k.

C. Fragmentation Analysis. To determine the fragmentation probabilities f_{nk}, it is necessary to specify both the deflection angle Θ and the final velocity v'. The easiest way to do this is to determine the velocity using a selector after the collision takes place. In this way, n is specified and then the different fragment masses k can be easily measured by the mass spectrometer.[7] In the present experimental arrangement, the velocity is measured by time-of-flight techniques so that we only know after the analysis which fragment mass belongs to which neutral cluster size. Although, in principle, the measured TOF signals N_{nk} contain all the information, it is much more convenient and accurate to use only the relative intensities of the TOF distributions X_{nk} given by

$$X_{nk}(\Theta) = N_{nk} / \sum_{n=k}^{n_{max}(\Theta)} N_{nk} \qquad (3)$$

and to relate them to the measured total scattered intensity $S_k(\Theta)$. Thus the probability f_{nk} for a neutral cluster of size n to fragment into an ion with mass k is given by

$$f_{nk} = N_{nk} / \sum_{k=1}^{n} N_{nk} \qquad (4)$$

By combining eqs 2 and 3 with eq 4 we get

$$f_{nk} = S_k X_{nk} / \sum_{k=1}^{n} S_k X_{nk} \qquad (5)$$

Here f_{nk} is expressed by two measurable quantities, S_k obtained from the differential cross section measurements and X_{nk} from the analysis of time-of-flight measurements of the scattered beam.

To get comparable values for the fragmentation probabilities, the parameters of the experimental setup must be known. A problem in this context is the transmission T_k of the quadrupole mass filter, which is not necessarily constant over the whole mass range. To ensure consistent and reproducible conditions during the whole series of measurements, the quadrupole mass spectrometer was calibrated using the known fragmentation pattern of the perfluorinated compound FC43.[29]

III. Results

For the determination of the fragmentation probabilities, we go through a three-step procedure: (1) A conventional mass spectrum is measured to learn about all relevant fragment channels k. (2) The total scattered intensity $S_k(\Theta)$ is obtained for deriving the optimal scattering angles Θ_n for each cluster size and for calibration purposes of the time-resolved signals. (3) Time-of-flight spectra are measured for each Θ and k for the determination of the relative intensities X_{nk}. For k the mass $m/z = 84$ u and the corresponding multiples were employed. The mass spectrum, taken at the electron energy of 70 eV, is dominated by peaks at the monomer and dimer ion mass, but also exhibits signals at other fragment Kr_n^+ ion masses with much smaller intensity.

We measured the angular dependent distributions $S_k(\Theta)$ at the seven fragment masses k with the largest intensities. The
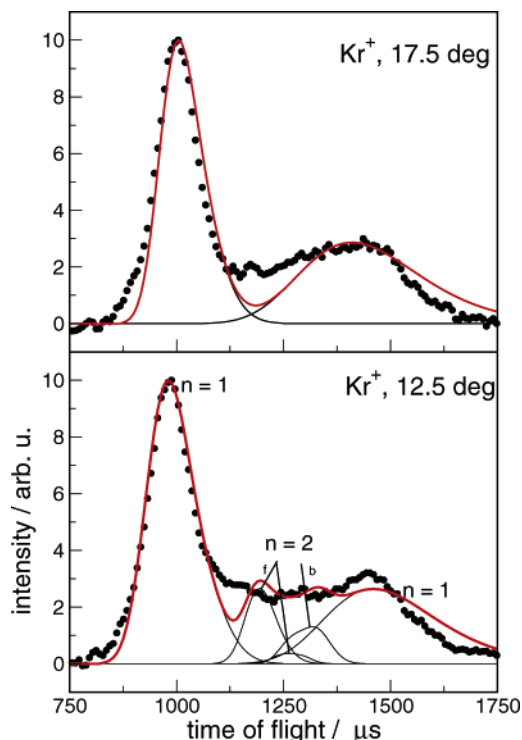

Figure 3. Measured time-of-flight distributions of the monomer (upper panel) and neutral dimer and monomer detected at the monomer mass Kr^+ (lower panel). The weak lines denote simulated contributions of the different neutral cluster sizes in the forward (f) and backward (b) direction for elastic scattering. For the dimer, also a small amount of inelastic scattering in the forward direction was accounted for.

results are shown in Figure 2. The colored shadows mark the theoretical limiting scattering angles Θ_n for the neutral cluster n, based on the beam data presented in Table 1 and broadened by the finite resolution of the apparatus. In general, the dominating fragment is the monomer ion (black). The onset of the dimer ion intensity (red) is in good agreement with the predicted limiting angle. The first contribution of the trimer ion (green) comes from the neutral pentamer. Fragment ions larger than the trimer ion contribute less than 1% of the total intensity for neutral Kr_n clusters up to $n = 7$.

To get information on the exact fragmentation probabilities, time-of-flight (TOF) spectra were measured at specified angles and masses in order to sort out the contributions of the different sizes. For that purpose, the measured data were compared with simulated TOF distributions. These distributions were obtained from Monte Carlo simulations, which take into account the special kinematics for the cluster scattering, the beam divergencies, the velocity distributions of the two beams, and the resolution of the TOF analyzer.[30] Then the calculated distributions were fitted to the measured spectra with the only adjustable parameter being the amplitudes, which are proportional to the effective elastic or inelastic cross sections. This procedure is best demonstrated for cases to which only a few species contribute. Two examples are shown in Figure 3. Here the experimental conditions concerning the deflection angle and the masses are such that only krypton monomers (17.5°) and monomers and dimers (12.5°) are detected. The weak lines indicate the contributions of the elastic forward and backward scattering which appear at shorter and longer times. For detection of the monomer ion in the upper panel, we observe two pronounced peaks, which correspond to deflection angles in the center of mass system of $\theta = 31°$ and $\theta = 160°$, respectively. In the lower part, the detection is still at the

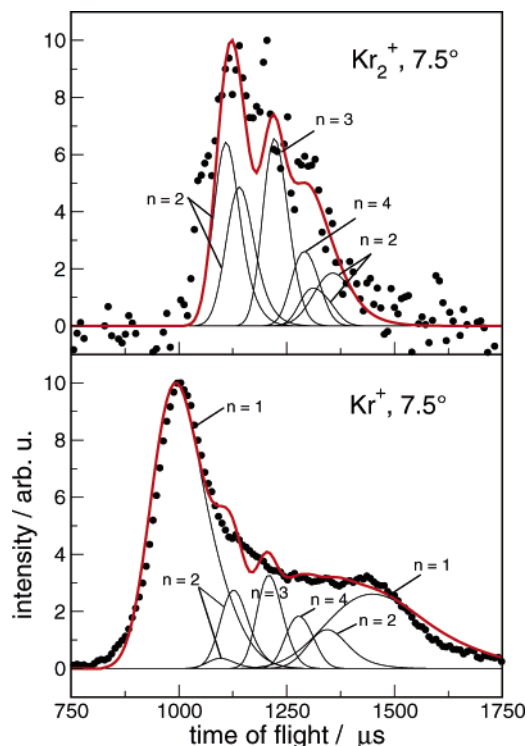**Figure 4.** Measured time-of-flight distributions of Kr_n-He scattering for the laboratory angle $\Theta = 7.5°$ taken at the monomer and dimer mass. The weak lines denote simulated contributions of the different cluster sizes. For the dimer, also inelastic contributions were accounted for. For clusters $n > 2$, only forward peaks are used in the fitting procedure.

monomer fragment mass, but now also neutral dimers contribute. They should appear, according to the Newton diagram, between the two limiting monomer peaks. For the dimer forward scattering, a small amount of inelastic contribution was necessary for a better reproduction of the measured curve in addition to the elastic scattering. It appears at smaller velocities and thus larger flight times.

To obtain the exact fragmentation probabilities of the larger neutral clusters, time-of-flight spectra have been measured at the angles 11°, 7.5°, 6°, 5°, and 4°. As an example, we show in Figure 4 the spectra taken at 7.5° together with fitted distributions of the different sizes for the two fragment masses Kr^+ and Kr_2^+. At this deflection angle pentamers are definitely ruled out. The contribution of tetramers is small but cannot be excluded because of the finite resolution of the apparatus. The fitted curves consist of the forward and backward scattering of monomers (where applicable) and dimers, and of the trimer and tetramer contributions in between. Aside from the dimer, the spectra could be well reproduced by elastic scattering. For the larger clusters, only the forward peak was fitted because of resolution problems. We note that this leads to lower limits of the corresponding fragmentation probabilities. By summing up all the simulated contributions, the measured spectra are well reproduced. Another example is shown in Figure 5 for the scattering angle of 5°. Here, the neutral clusters $n = 5$ and $n = 6$ can also contribute. We observe again the forward and backward peaks of the monomer and the dimer for the Kr^+ detection (lower part) and those of the dimer for the Kr_2^+ detection (upper part). For the larger clusters again only one peak was fitted. Similar results have been obtained for the other deflection angles in which cluster sizes up to $n = 7$ have been included. From these data, the relative contributions of the TOF data X_{nk} are obtained. They have to be calibrated by the
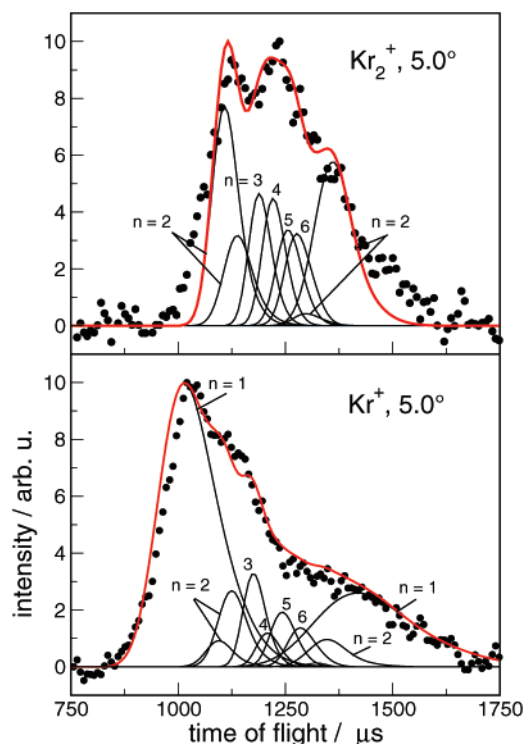
Figure 5. Measured time-of-flight distributions of Kr_n-He scattering for the laboratory angle $\Theta = 5.0°$ taken at the monomer and dimer mass. The weak lines denote simulated contributions of the different cluster sizes. For details see Figure 4.

TABLE 2: Total Scattered Intensity S_k (see Figure 2) Detected at the Ion Mass k for the Angles for Which TOF Data Were Taken

Θ (deg)	$k=1$	$k=2$	$k=3$	$k=4$	$k=5$	$k=6$	$k=7$
12.5	5842	46					
11.0	6506	67					
7.5	8872	89					
6.0	10965	117	2				
5.0	13188	170	9	3	2		
4.0	16737	288	38	6	4	4	2

TABLE 3: Fragmentation Probabilities f_{nk} of the Cluster Size n to the Ion Size k

n	$k=1$	$k=2$	$k=3$
2	0.951(13)	0.049	
3	0.973(13)	0.027	
4	0.961(20)	0.039	
5	0.965(14)	0.029	0.006
6	0.926(18)	0.053	0.021
7	0.902(12)	0.063	0.035

corresponding intensities of the total differential cross sections S_k from Figure 1; the relevant values are listed in Table 2. The final results of the fragmentation probabilities, averaged over the contributions from different angles, are presented in Table 3.

The experimental results obtained in the early stage of the experiment with the other apparatus are quite similar. The total scattered intensity as a function of the deflection angle exhibits the same behavior as that shown in Figure 2. By far the largest signal is that of the monomer ion Kr^+, followed by the dimer signal Kr_2^+ and the rest of the ions. A similar behavior is observed for the TOF distributions. As an example, we show in Figure 6 the fitted TOF spectrum of the Kr_2^+ and Kr^+ fragments measured at the laboratory angle of 7.0°. Despite the different geometries (note the flight times are twice as long)
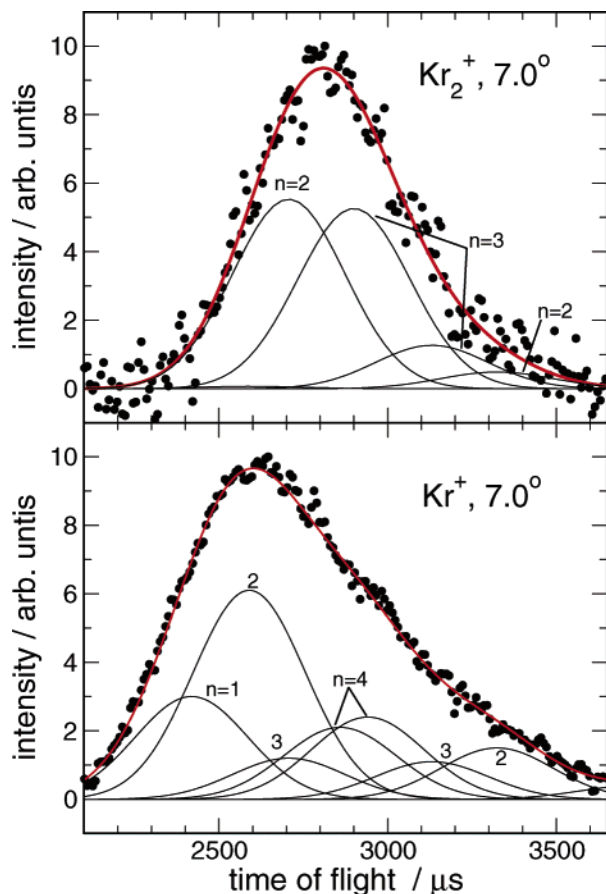
Figure 6. Measured time-of-flight distributions of Kr$_n$-He scattering for the laboratory angle $\Theta = 7.0°$ taken at the dimer (upper panel) and the monomer mass (lower panel). The data are taken in a different molecular beam machine described in the text. The weak lines denote simulated contributions of the different cluster sizes.

the spectrum resembles the one in Figure 4, measured at an angle of 7.5° in the present apparatus. Because of the lower resolution, the spectrum in Figure 6 could only be fitted by peaks corresponding to the neutral sizes $n = 2$ and 3. The contribution of $n = 4$ at the angle above the threshold for the tetramer $\Theta_4 = 6.5°$ was neglected. Also the inelastic scattering used for $n = 2$ in the fits in Figure 4 was omitted although it is implicitly included in the fitted peak width in Figure 6. A whole series of measurements similar to the above ones at different angles was carried out in this apparatus. The analysis gives fragmentation probabilities as follows: dimer, $f_{21} = 0.992$ and $f_{22} = 0.008$; trimer, $f_{31} = 0.938$ and $f_{32} = 0.062$; and tetramer, $f_{41} = 0.960$ and $f_{42} = 0.040$. Despite the lower resolution, they agree with the ones in Table 3 to within a few percent. This comparison with an independent and quite different experiment (in geometry) provides a confirmation of the measured fragmentation probabilities.

Given the complicated nature of the extraction of branching ratios from the data, involving integration over eleven variables, it is difficult to extract precise error bars from the analysis. Perhaps the greatest source of error is illustrated in Figure 3. Although the data collected at 17.5° should have only minor contributions from neutral dimer ionization, there is still significant intensity between the two expected monomer peaks. This may result in an overestimate of the fraction of neutral dimer that fragments to monomer ions. Our best estimate is that the lower limit for this fraction is 90%, as opposed to the value of 95% that results from the best fit to the data.

IV. Discussion

The results presented above were quite surprising to us, and that is why we repeated the initial experiments on a second scattering machine that yields more precise results. There was no obvious reason to expect that argon and krypton clusters should fragment differently upon electron impact ionization. In the case of argon clusters, $2 \leq n \leq 9$, the main fragment ion was always the strongly bonded Ar$_2^+$ dimer ion. This was already surprising since the Ar$_3^+$ trimer ion is also quite stable. In the case of krypton clusters, we find that the fragmentation pattern is dominated by the Kr$^+$ monomer for initial neutrals with $n \leq 7$. Since this result is so unexpected, we will discuss the details of the experiment and possible sources of error in some detail.

First we discuss the influence of collisional induced dissociation on the measured fragmentation probabilities. To get an estimate of the transferred energy in the collision of the Kr$_n$ cluster with He, we apply the impulsive model proposed by Mahan.[31] In this model the collision of the scattering partner He (mass m_s) with one Kr atom of the cluster (mass $n\,m_c$) is considered, neglecting the bonds. The energy transfer ΔE is given in terms of the collision energy E by

$$\frac{\Delta E}{E} = \frac{4(m_c + m_s/n)m_s}{(m_s + m_c)^2}\left(1 - \frac{1}{n}\right) \qquad (6)$$

For the 64 meV collision energy, the energy transferred to the neutral cluster amounts to 5.8 meV for Kr$_2$ and 9.5 meV for Kr$_7$. The dissociation energy for the dimer is 15.9 meV with the zero-point energy included. For the heptamer, the same value per atom is 37.3 meV.[13] Thus, it is unlikely that collisional energy transfer explains the surprisingly large degree of fragmentation. This conclusion is supported by the recent calculations of Halberstadt and co-workers,[13] who investigated the effect of adding an additional 10.1 meV energy to the Kr$_6$ fragment and found the effect to be negligible. These calculations suggest that collisional excitation of the neutral clusters does not significantly affect the results presented here, but it would be useful to examine this assumption in greater detail, especially for the smaller neutral clusters, perhaps with realistic simulations of the scattering process.

In particular, one expects that collisional excitation should be less important for the present study of krypton clusters than for the previously reported results of argon clusters. For the argon clusters, fragmentation of the neutral dimer and trimer was investigated[6] using the same experimental arrangement as used to obtain most of the findings presented here, while the higher clusters were studied[7] with the apparatus used to obtain the preliminary krypton results shown in Figure 6. The main difference between the argon and krypton cluster experiments is that the mass of argon is less than that of krypton, so the Newton diagram is a bit more expanded for argon, leading to slightly better separation of the neutral clusters in angle and time. The results for argon and krypton clusters are similar in the sense that fragmentation is extensive for both species, with the trimer ion first appearing for ionization of the neutral pentamer in each case. So, the main difference between the two studies is that ionization of small argon clusters leads mainly to the production of the Ar$_2^+$ dimer ion, ranging from 70% for $n = 3$ to 51% for $n = 9$, while ionization of small krypton clusters results dominantly in the Kr$^+$ monomer ion, ranging from 97% for $n = 3$ to 90% for $n = 7$. This aspect of the results was completely unexpected, but the data presented in Figures 2−6 is quite unambiguous.

Fragmentation of Krypton Clusters

J. Phys. Chem. A, Vol. 110, No. 29, 2006 **9113**

In addition to their masses, another difference between Ar and Kr is that there are more electronic states accessible by electron impact excitation for Kr than for Ar, the ionization cross sections for the two species will also be somewhat different, and the spin−orbit excitation energy for the ground ionic state is significantly larger for Kr^+ than for Ar^+. There is limited information available for these effects on the dimer ions, and almost no information available for the larger cluster ions. Ab initio calculations of the electron impact excitation cross sections indicate that the probabilities of excitation to electronic states higher than the valence states are quite low for bare atoms.[32] Since the effects observed here are dramatic, they are probably not due to excitation to high-energy electronic states. Although we do not know how clustering will affect this conclusion, we do not expect that the effects would be strong enough to explain the surprising results presented above.

Spin−orbit coupling is likely to be a more important effect. Spin−orbit excitation of Kr^+ is almost 4 times as energetic as for Ar^+; 0.67 versus 0.18 eV, respectively. Spin−orbit coupling is also known to have a qualitative effect on the dimer ion potential curves. This is most dramatic for the I ($^1/_2$g) state which has a 550 cm^{-1} deep well at $r_e = 3.047$ Å for Ar_2^+, but only a 50 cm^{-1} deep well at $r_e = 6.11$ Å for Kr_2^+. The I ($^3/_2$u) and II ($^1/_2$g) potentials for Kr_2^+ are also somewhat less attractive than that of Ar_2^+. Thus it might have been expected that ionization of Kr_2 has a greater propensity to yield Kr^+ than does the comparable ionization of Ar_2. In this regard, it is interesting to note that recent calculations by Bonhommeau et al.[33] of the fragment branching for ionization of Ar_2 employing a mixed quantum-classical dynamics model that includes spin−orbit coupling is in good agreement with the data: the calculation predicts 35% branching to Ar^+ compared to an observed value of 40%. Similar calculations for Kr_2 predict 50% branching to the monomer compared to the 95% observed. In this regard the calculation predicted the correct trend, but not the surprising dominance of the monomer ion for neutral dimer ionization.

As mentioned above, Bonhommeau et al. have performed simulations of the noble gas cluster fragmentation upon ionization for Ne_n, Ar_n, and Kr_n clusters.[12,13,33] The calculations predict that in all three cases the Rg_2^+ dimer ion is the most probable fragmentation channel up to the largest clusters studied, $n = 11$ in the case of argon. In the case of argon cluster fragmentation the calculations are in qualitative accord with the experimental results, although the details showed some differences. For instance, the calculated production of Ar^+ from ionization of Ar_n fell monotonically with n, whereas the experimental results did not produce such a smooth trend. The experimental Ar^+ fraction was larger than the calculated value for all cluster sizes. Given the difficulty of both the experiments and calculations, the level of agreement can be considered to be quite good for argon cluster ionization/fragmentation.

When we compare the experimental results of this paper for Kr_n cluster fragmentation with the calculations,[13] we first observe an agreement in the general observation of an extensive fragmentation and in the appearance of the trimer ion channel. This is demonstrated in Figure 7, where the fragmentation probabilities for the trimer ion f_{n3} and the sum of that for the monomer and the dimer ion $f_{n1} + f_{n2}$ are plotted. The figure also contains the results without spin−orbit interaction. While the results for the larger clusters do not differ very much from those with spin−orbit interaction included, there is a pronounced difference for the neutral trimer. An appreciable fraction of Kr_3^+ originates from the existence of a minimum in one of the electronic states close to the equilibrium configuration of the
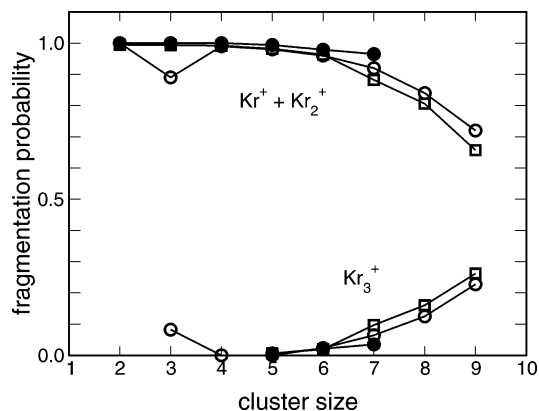

Figure 7. Comparison of measured and calculated fragmentation probabilities for the sum of $f_{n1} + f_{n2}$ and f_{n3} for Kr_n from $n = 2$ to 9: experiment, closed symbols; calculation, open symbols; circles, without spin−orbit interactions; squares, with spin−orbit interactions.

neutral cluster, which disappears when the spin−orbit interaction is included[13] and agrees with experiment. If we, however, look at the direct comparison of the fragmentation probabilities f_{n1} and f_{n2} into the monomer and the dimer ion channel, the agreement is less good. The calculations predict that 50% of Kr_2 dimers fragment to Kr^+ monomers upon ionization, and this fraction drops rapidly with increasing neutral cluster size. For $n > 4$, the calculated probability of observing the Kr^+ monomer ion is always less than 20%, whereas the experimental value remains close to 90% up to $n = 7$, the largest neutral studied. Similar discrepancies occur for the fragmentation probabilities f_{n2} of the dimer ion. Here the calculated values increase from 49% for $n = 2$ to a maximum at 84% for $n = 6$ and then drop again to 63% for $n = 9$, while the experimental values oscillate between 2.7% and 6.3%. There is good agreement between experiment and theory as for the strong fragmentation into monomer and dimers ions, but the main disagreement is specifically the branching ratio between monomer and dimer ions. We note that including the spin−orbit excited states in the calculation significantly increase the calculated fragmentation to the Kr^+ monomer for $n = 2$ and 3. This effect is masked in Figure 7 by the simultaneous decrease of the fragmentation probability for dimer ions. Given that the effects of spin−orbit excitation double the calculated probability of obtaining Kr^+ monomer ions from ionization of the neutral dimer, it may be worth further exploring the details of the excitation cross sections to spin−orbit excited states to improve the agreement between experiment and theory.

Let us discuss the possible errors of the experiment with respect to the calculations. The experiments consist of the measurement of two quantities, the relative intensities of the TOF distributions X_{nk}, and the total scattered intensities S_k both as function of the deflection angle. In the results section we discussed one possible reason the analysis of the experiment may have overestimated the fragmentation to the Kr^+ monomer ion; leakage of signal from neutral monomers into the space-time scattering domains expected to be dominated by neutral dimers. However, as discussed above it is highly unlikely that this would make more than 5% difference in the fraction of observed Kr^+. This is also confirmed by comparing the results obtained in the two different experimental arrangements, which deviate by 4% at most. Therefore these effects are not able to explain the large discrepancies with the calculations.

Another possible source of experimental error is the secondary ionization of neutral fragments which are products of the primary ionization. The calculations demonstrate that for each neutral

cluster size, aside from the ionic fragments, also about $n - 2$ neutral monomer fragments are generated. Provided that these Kr atoms are also ionized by the electrons of the ion source, the intensity of the monomer ions will increase appreciably. This number affects both the total intensities S_1 and the X_{n1} values of the time-of-flight distributions and increases with increasing cluster size. A tentative correction of this effect leads in fact to a decrease of the monomer ion contribution, especially for the larger clusters, but the resulting fragmentation probabilty for the dimer ion f_{n2} is still too low by about 30%. In addition, the fragmentation probabilty for the trimer ions f_{n3} yields rather large, unrealistic values (9−35%). Therefore we discard this correction to be responsible for the discrepancies, also in view of the fact that the smaller clusters are not at all or only weakly influenced by this effect.

A drawback of the calculation is apparently the time scale of the trajectories. Most of them range up to 100 ps and some of them reach 10 ns. The latter ones are included in the calculations in the "long-lived trajectories." In the experiment, however, time scales in the order of μs are available for the ions on their way from the ion source to the entrance of the quadrupole. It could very well be that this might lead to further evaporative processes resulting in Kr$^+$, although the preference of the calculated "long-lived trajectories" at shorter time scales for larger clusters weakens this argument.

A further interesting issue is the role of the excited states. In the calculation it is assumed that all excited states of the parent ion Kr$_n^+$ are equiprobably populated. The calculations for selected sizes, however, show that monomer fragments originate preferentially from trajectories initiated in the highest electronic states.[13] In the case of Kr$_8^+$ this contribution amounts to 20%, while the average fragmentation probability is 1% under otherwise similar conditions. Interestingly, this difference disappears for argon clusters as was demonstrated for Ar$_9$ in ref 33. A careful inspection, however, shows that for smaller clusters the discrepancies between krypton and argon clusters disappear and it is also not conceivable why special states should be selected in the ionization process.

After extensive analysis of the experiment and careful reading of the theory manuscripts, we are left with the conclusion that there is a real disagreement regarding the branching ratio to monomer and dimer ions. Necessarily, theory on such a complicated problem involves a variety of approximations. The work of Halberstadt and co-workers employs a diatomics-in-molecule (DIM) potential which is expected to be reasonably accurate for the valence states. Nuclear motion is treated classically, and transitions between states of the ion are made statistically on the basis of quantum mechanical probabilities. One obvious approximation in any such calculation is the difficulty in properly treating zero-point energy in a classical calculation. Ironically, experiment and theory are in better accord for argon clusters than krypton clusters, so it is unlikely that the classical approximations are the major source of disagreement. In this regard we note that the experiment and theory are already in substantial disagreement for ionization of the krypton dimer. So, we hope that it might be possible to perform less approximate calculations for the dimer species to investigate the effects of the approximations made in the calculations by Bonhommeau et al.[13] and perhaps also to incorporate some of the details of the experiment in the simulation. One example of such a detail that might be more important than expected is the effect of excitation of the neutral dimers by the size selection-scattering event. It would also be very interesting to investigate the effects of spin−orbit excitation on the ionization cross sections for the larger neutral clusters.

V. Conclusions

We have reported results of a study of the ionization and fragmentation of neutral krypton clusters up to Kr$_7$ by electron impact. For each initial cluster size the probability of branching to monomer Kr$^+$ ions is much higher than expected on the basis of a previous study of argon cluster ionization. Calculations by Bonhommeau et al.[13] also predict more monomer ion product for krypton clusters than for argon clusters, because of the effect of the larger spin−orbit excitation energies in the krypton cluster ions. However, the effect is much smaller in the calculations than for the experimental results. On the other hand, the calculations and the experiments are in accord regarding the fact that Kr$_3^+$ ions first start to appear for the ionization of neutral pentamers. Given that the results presented here are so surprising, and contrary to the current best calculations, we have discussed possible sources of error in considerable detail.

References and Notes

(1) Barker, J. In *Rare Gas Solids, Vol. I*; Klein, M. L., Venables, J. A., Eds.; Academic Press: New York, 1976; page 212.

(2) Haberland, H. *Surf. Sci.* **1985**, *156*, 305.

(3) Buck, U. In *The Chemical Physics of Atomic and Molecular Clusters*; Scoles, G., Ed.; North-Holland: Amsterdam, The Netherlands, 1990; page 543.

(4) Märk, T. D.; Echt, O. In *Clusters of Atoms and Molecules II*; Haberland, H., Ed.; Springer: Berlin, Germany, 1994; page 154.

(5) Buck, U.; Meyer, H. *Phys. Rev. Lett.* **1984**, *52*, 109.

(6) Buck, U.; Meyer, H. *J. Chem. Phys.* **1986**, *84*, 4854.

(7) Lohbrandt, P.; Galonska, R.; Kim, H.-J.; Schmidt, M.; Lauenstein, C.; Buck, U. In *Atomic and Molecular Beams*; Campargue, R., Ed.; Springer: Berlin, Germany, 2001; page 623.

(8) Bastida, A.; Halberstadt, N.; Beswick, J. A.; Gadéa, F. X.; Buck, U.; Galonska, R.; Lauenstein, C. *Chem. Phys. Lett.* **1996**, *249*, 1.

(9) Kuntz, P. J.; Valldorf, J. *Z. Phys. D: At., Mol. Clusters* **1988**, *8*, 195.

(10) Ikegami, T.; Kondow, T.; Iwata, S. *J. Chem. Phys.* **1993**, *98*, 3038.

(11) Bonhommeau, D.; Viel, A.; Halberstadt, N. *J. Chem. Phys.* **2004**, *120*, 11359.

(12) Bonhommeau, D.; Viel, A.; Halberstadt, N. *J. Chem. Phys.* **2005**, *123*, 54316.

(13) Bonhommeau, D.; Bouissou, T.; Halberstadt, N.; Viel, A. *J. Chem. Phys.* **2006**, *124*, 164308.

(14) Thissen, R.; Lablanque, P.; Hall, R. I.; Ukai, M.; Ito, K. *Europ. Phys. J. D* **1998**, *4*, 335.

(15) Hatsui, T. *J. Chem. Phys.* **2005**, *123*, 154304.

(16) Malone, C.; Kedzierski, W.; McConkey, J. W. *Eur. Phys. J. D* **2002**, *18*, 87.

(17) Hiraoka, K.; Mori, T. *J. Chem. Phys.* **1990**, *92*, 4408.

(18) Parajuli, R.; Matt, S.; Echt, O.; Stamatovic, A.; Scheier, P.; Märk, T. D. *Chem. Phys. Lett.* **2002**, *352*, 288.

(19) Ha, T.-K.; Rupper, P.; Wüest, A.; Merkt, F. *Mol. Phys.* **2002**, *101*, 827.

(20) Gulch, K.; Matt-Leubner, S.; Michalek, L.; Echt, O.; Stamatovic, A.; Scheier, P.; Märk, T. D. *J. Chem. Phys.* **2004**, *120*, 2686.

(21) Buck, U.; Lauenstein, C.; Meyer, H.; Sroka, R. *J. Phys. Chem.* **1988**, *92*, 1916.

(22) Buck, U.; Lauenstein, C.; Sroka, R.; Tolle, M. *Z. Phys. D: At., Mol. Clusters* **1988**, *10*, 303.

(23) Buck, U.; Hoffmann, G.; Kesper, J.; Otten, D.; Winter, M. *Chem. Phys.* **1988**, *126*, 159.

(24) Beneventi, L.; Casavecchia, P.; Rusin, L. Y.; Volpi, G. G. In *The Chemical Physics of Atomic and Molecular Clusters*; Scoles, G., Ed.; North-Holland: Amsterdam, The Netherlands, 1990; page 579.

(25) Buck, U.; Lauenstein, C. *J. Chem. Phys.* **1990**, *92*, 4250.

Fragmentation of Krypton Clusters

J. Phys. Chem. A, Vol. 110, No. 29, 2006 **9115**

(26) Buck, U.; Winter, M. *Z. Phys. D: At., Mol. Clusters* **1994**, *31*, 291.

(27) Buck, U.; Huisken, F.; Schleusener, J.; Schäfer, J. *J. Chem. Phys.* **1980**, *72*, 1512.

(28) Baumfalk, R.; Buck, U.; Frischkorn, C.; Gandhi, S. R.; Lauenstein, C. *Ber. Bunsen-Ges. Phys. Chem.* **1997**, *101*, 606.

(29) Busch, K. L. *Spectroscopy* **2005**, *20*, 20.

(30) Buck, U. In *Atomic and Molecular Beam Methods*; Scoles, G., Ed.; Oxford University Press: New York, 1988; page 525.

(31) Mahan, B. H. *J. Chem. Phys.* **1970**, *52*, 5221.

(32) Bartlett, P. L.; Stelbovics, A. T. *Phys. Rev. A: At., Mol., Opt. Phys.* **2002**, *66*, 012707.

(33) Bonhommeau, D.; Halberstadt, N.; Viel, A. *J. Chem. Phys.* **2006**, *124*, 184314.